Direct method of surface structure determination by Patterson analysis of correlated thermal diffuse scattering for Si(001)2x1

Direct method of surface structure determination by Patterson analysis of correlated thermal diffuse scattering for Si(001)2×1

T. Abukawa,[1] C. M. Wei,[2] K. Yoshimura,[1] and S. Kono[1]
[1]*Research Institute for Scientific Measurements, Tohoku University, Sendai 980-8577, Japan*
[2]*Institute of Physics, Academia Sinica, Nankang, Taipei, Taiwan 11529, Republic of China*
(Received 27 December 1999; revised manuscript received 5 June 2000)

A simple oscillatory intensity variation in medium-energy electron diffraction found recently [Abukawa *et al.*, Phys. Rev. Lett. **82**, 335 (1999)] was termed correlated thermal diffuse scattering (CTDS). The potential of CTDS as a direct surface structural tool has been fully explored for the Si(001)2×1 surface at 300 K in a very-grazing-incidence condition. Nearly 2π solid-angle, three-dimensional (3D) CTDS patterns were measured for an energy range of 500–2000 eV. The 3D Patterson functions obtained by Fourier inversion of the measured CTDS patterns clearly revealed the building blocks of the Si(001)2×1 surface, i.e., the bond orientations and lengths of the buckled Si dimers, within an accuracy of 1° and 0.1 Å, respectively.

In contrast to the reliable routine techniques in bulk crystallography, no counterparts are available in surface crystallography. One obvious reason is the absence of a kinematical diffraction technique that leads to a direct method of surface structure determination. Although surface x-ray diffraction (SXRD) is a kinematical structural tool, it is experimentally difficult to measure a sufficient number of surface reflection intensities and most of the Patterson functions obtained are two-dimensional projections onto the surface plane, even when using a brilliant synchrotron radiation source. The development of a direct method in surface crystallography has been of the highest priority in surface science.[1–7] Very recently, we described a feature in the thermal diffuse scattering (TDS) of medium-energy electron diffraction (MEED) that could be considered as an approximate kinematical diffraction feature.[8] The observed feature is due to strong vibrational correlation among near neighbor atoms; it is called correlated thermal diffuse scattering (CTDS), and may have the same origin as the TDS streaks known in transmission electron diffraction (TED). The feature can be used as a direct method of surface crystallography based on three-dimensional (3D) Patterson analysis when grazing electron incidence is used. Since a laboratory electron source is used for the measurement, it is rather easy to collect a sufficient number of data sets to create the 3D Patterson function of the surface structure. This is a great advantage over SXRD, in which usually a two-dimensional projection of the Patterson map is available from a limited number of data sets. Here we have fully exploited the method of CTDS Patterson analysis on a clean Si(001)2×1 surface. The surface structure of Si(001)2×1, i.e., the bond length and orientation of buckled dimers and the relaxation under the dimers, has been directly reconstructed within an accuracy of 0.1 Å, in good agreement with reliable previous values. This demonstrates that the CTDS Patterson analysis is a promising direct method of surface structure determination.

It is known that the TDS intensity shows broad peaks at the Bragg spots or broad streaks between the Bragg spots since the vibrations of crystal atoms are correlated within a short range.[9–13] Recently, the TDS streaks in TED have been analyzed by semiclassical theory as well as by quantum mechanical theory.[11–13] In brief, the TED TDS pattern can be expressed by the convolution of the dynamical elastic diffraction pattern with the kinematical TDS scattering function. The kinematical TDS scattering function is caused by the short-range coherency created by phonon scattering, that is, the vibrational phase correlation. It is also shown that coherency between the first nearest neighbors (NN's) gives a large contribution and qualitatively reproduces the features of TED TDS streaks. Although the theory for TED might not be directly applicable to the present MEED, strong vibrational coupling between NN's must play a similar important role in MEED TDS.

We first estimate the degree of vibrational correlation between the NN atoms by calculating the mean square relative displacement (MSRD) of bulk Si using a theory developed for extended x-ray-absorption fine structure analysis.[14] The solid curve in Fig. 1 represents the calculated MSRD for Si at 300 K as a function of the interatomic distance. Although a correlated Debye model was used for simplicity, the result should show the qualitative features of the result of the more

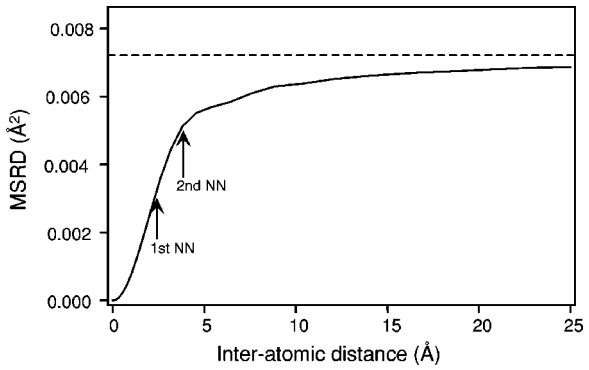

FIG. 1. Mean square relative displacement of Si atom in bulk Si at 300 K as a function of the interatomic distance as calculated from a correlated Debye model (Ref. 14). Arrows indicate MSRD's at the first NN and second NN distances. Horizontal broken line is for the uncorrelated MSRD which is twice the individual mean square displacement.

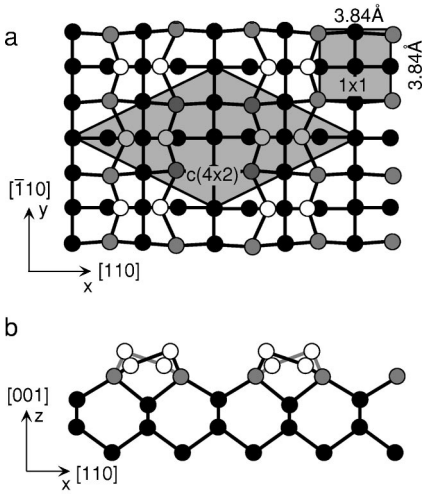

FIG. 2. Ball-and-stick model for the Si(001)$c(4\times2)$ surface; (a) top view; (b) side view from $[1\bar{1}0]$ direction. Only the top five layers are shown. Open, gray, and solid circles are Si atoms of the top layer, the second layer, and below, respectively. The top layer Si atoms are dimerized and the ones below the dimers are relaxed from the ideal bulk positions. The unit cells of $c(4\times2)$ and 1×1 are shown in the top view.

realistic phonon model.[14] The horizontal broken line in Fig. 1 indicates the uncorrelated MSRD, which is twice the individual mean square displacement of bulk Si at 300 K. The MSRD in Fig. 1 slowly decreases with decrease in the interatomic distance to ~5 Å but sharply decreases from there. The MSRD for the nearest neighbor bond length ($r=2.35$ Å) and that for the second NN atoms ($r=3.84$ Å) are reduced to 45% and 70% of the uncorrelated MSRD values, respectively. Thus, it is probable that the coherency between the nearest neighbor atoms survives even at high angle scattering and causes the streaks in TED or CTDS in MEED. Strong NN coupling should be expected even at the surface, although the vibration is rather different between surface and bulk.

The structure of the Si(001)2×1 surface has been semiquantitatively determined at last by investigations using various surface structural techniques.[15–19] This surface has a nominal 2×1 periodicity at room temperature (RT) but a $c(4\times2)$ periodicity at low temperature (LT), as schematically shown in Fig. 2. At RT, the LT long-range order of $c(4\times2)$ disappears but the local structure of dimer buckling is intact, resulting in the nominal Si(001)2×1 surface.[19]

A single-domain Si(001)2×1 surface[20] was prepared in an ultrahigh vacuum chamber [see Fig. 3(a)], which was equipped with a microbeam electron gun designed for a scanning electron microscope, a retarding field display analyzer (RFDA), and reflection high-energy electron diffraction (RHEED) optics.[21] The RFDA displays the angular distribution of electron intensity up to 3 keV of primary energy with a cone angle of 74° and has enough energy resolution ($E/\Delta E\approx600$) to resolve elastically scattered electrons from electrons undergone plasmon and higher-energy losses. The retarding field analyzer energy was set at the valley between the elastic peak and the plasmon loss peak, i.e., about 5 eV below the incident beam energy. As phonon losses were involved in the detected electrons, the detected electrons are

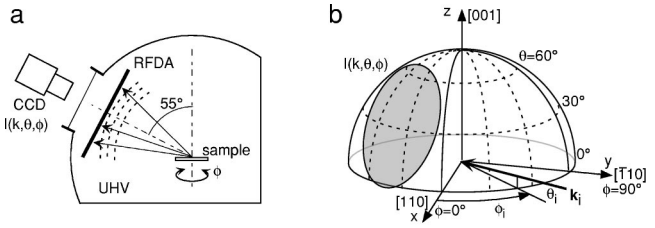

FIG. 3. (a) Schematic illustration of the apparatus. A microelectron beam was incident along the direction perpendicular to the paper onto the sample surface at a grazing angle. The quasielastically scattered electrons were detected by the RFDA consisting of three spherical grids and a micro-channel plate assisted phosphorus screen. The screen image was measured by a charge-coupled device (CCD) video camera. (b) The coordinates of the measurement. The sample surface is in the xy plane and the dimer rows of single-domain sample are arranged as in Fig. 2. The vector $\mathbf{k}_i$ is the incident vector and the detection solid angle of the RFDA is shaded. The relationship between $\mathbf{k}_i$ and the RFDA was fixed, and the sample was rotated about the surface normal in order to expand the detection zone.

called ''quasielastically'' scattered electrons hereafter.

The experimental method of CTDS could be called grazing-incidence backscattering medium-energy electron diffraction.[21] A medium-energy electron beam was incident onto the sample surface at a very grazing angle θ_i of 3°, instead of 10° in the previous study,[8] to increase the surface sensitivity [see Fig. 3(b)]. The angular (θ,ϕ) distribution of quasielastically backscattered electron intensity was measured as a function of primary electron wave number k from 11.34 to 22.68 Å^{-1} at equal intervals of 0.378 Å^{-1} (the electron energy being from 490 to 1959 eV), keeping the incident angle, θ_i constant. Thus, 31 screen images with dif-

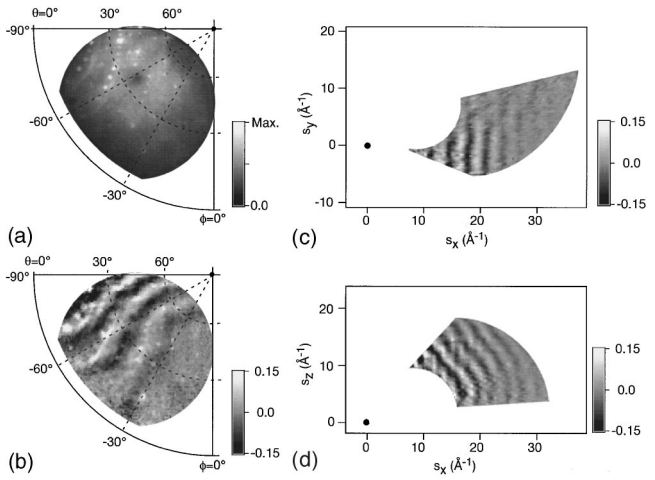

FIG. 4. (a) A typical raw screen image of quasielastically scattered electron intensity as measured by the RFDA for an incident electron energy $E_P=728$ eV ($k=14.74$ Å^{-1}) and incident azimuth $\phi_i=45°$. The scale bar shown is normalized to its maximum intensity. (b) A CTDS pattern processed from (a). The scale represents a normalized oscillation (see text). (c) Horizontal section at $s_z=9.0$ Å^{-1} of the 3D χ function for $\phi_i=45°$ mapped in the reciprocal space. (d) Same as in (c) but vertical section at $s_y=0.0$ Å^{-1}. A dot is placed at the origin as a guide for the eye in (c) and (d).

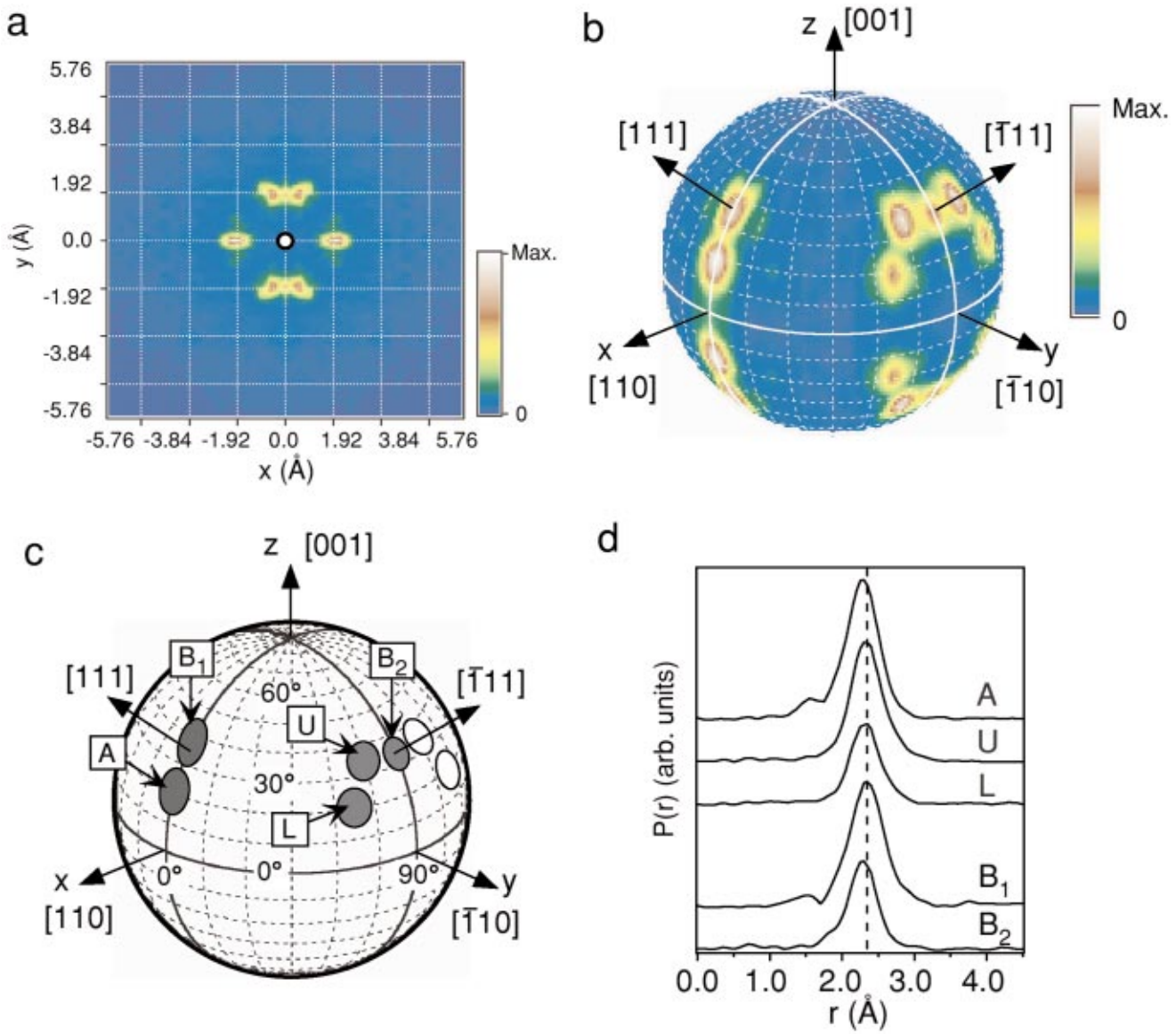

FIG. 5. (Color) (a) Projection of the 3D Patterson function $P(\mathbf{r})$ onto the xy (surface) plane of Si(001)2×1. A linear color scale is shown on the right. The grid spacing corresponds to one-half of the 1×1 unit cell. An open circle is placed at the origin for clarity. The vector to each intense spot from the origin corresponds to the projection of an interatomic vector (see text). (b) Spherical section of $P(\mathbf{r})$ at $r=2.35$ Å (Si-Si bond length in bulk). Polar and azimuth angular grids together with a linear color scale bar are shown. (c) Assignment of the distinct spots in (b). There are three surface specific spots A, U, and L, and two bulk related spots B_1 and B_2 (see text). (d) Radial profiles of $P(\mathbf{r})$ along the direction passing the center of the five spots. The curves are offset along the ordinate for clarity. The vertical dashed line marks the ideal Si-Si bond length of 2.35 Å.

ferent k values were obtained at one incident orientation (a single 3D data set). The measurement typically took 80 min. One of the raw screen images is shown in Fig. 4(a). The raw screen image is modulated by the inhomogeneous sensitivity of the RFDA and is overlapped by weak Bragg spots. The Bragg spots were very weak, but still brighter than in TDS at this relatively low kinetic energy. However, we can filter out the inhomogeneous sensitivity and the Bragg spots, and pick up the normalized intensity oscillation along the k direction from the 3D data set using the normalization procedure mentioned in Ref. 6. In order to extract the oscillation components, we used a fast Fourier transformation filter instead of the original polynomial fitting method in Ref. 6. After the normalization, a 3D normalized oscillation χ was obtained from the single 3D data set. A constant energy slice of the 3D χ function, which is processed from Fig. 4(a), is shown in Fig. 4(b). As the angular inhomogeneous sensitivity has been compensated, a simple wavy pattern, which is a typical CTDS pattern, has become clear. The trace of Bragg spots visible in Fig. 4(b) makes a negligible contribution to the large volume of the observed 3D data set. It should be pointed out here that the presence of clear RHEED 2×1 patterns (not shown) indicates the well-ordered surface structure of the present sample. However, one may consider that minor static disorder may cause a wavy pattern as in Fig. 4(b). This can be safely denied, since medium-energy electron diffraction is used at large scattering angles, which makes the thermal diffuse scattering very dominant.

The aspect of the whole 3D χ function becomes clearer in reciprocal space. Thus, the 3D χ function was converted into

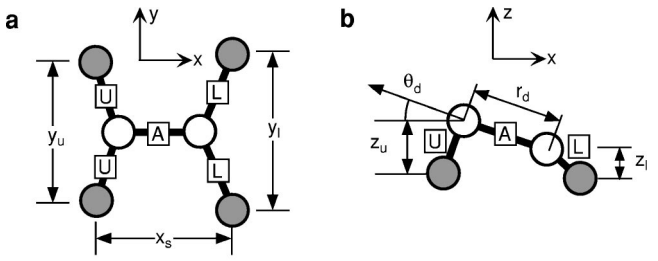

FIG. 6. Ball-and-stick model of an asymmetric dimer unit: (a) top view; (b) side view from the $[1\bar{1}0]$ direction. The assignments of distinct spots in Fig. 5(c) and the structural parameters obtained in the present study are indicated.

the reciprocal coordinate of the scattering vector, $\mathbf{s}=\mathbf{k}-\mathbf{k}_i$, where $\mathbf{k}$ and $\mathbf{k}_i$ are the wave vectors of scattered and incident electrons, respectively. Two slices of the 3D χ function obtained in reciprocal space are shown in Figs. 4(c) and 4(d). The waves are evenly spaced, which is characteristic of a cosine wave. This indicates that the waves are caused by pairs of atoms.[8] The direction and frequency of the wave should be related to the interatomic direction and the interatomic distance, respectively. They will be directly reconstructed as the Patterson function by Fourier transformation.[8]

As mentioned in the previous study,[8] only the atomic pairs whose interatomic vectors are nearly parallel to the measured reciprocal angular range are observable in the Patterson function of CTDS. Therefore, we measured 3D CTDS patterns at nine different incident azimuths to expand the survey volume into a quadrant of full azimuth range. Then the quadrant was extended to full azimuth range taking into account the surface symmetry, i.e., twofold symmetry with two mirror planes or C_{2v} symmetry. The increase in the surveyed volume improves the real space resolution as well. Finally, the whole 3D χ function in reciprocal space was Fourier transformed into a single 3D Patterson function $P(\mathbf{r})$.

The projection of the 3D Patterson function $P(\mathbf{r})$ onto the xy (surface) plane is shown in Fig. 5(a), which shows distinct spots over a very low noise level. The vector to each distinct spot from the origin would correspond to the xy projection of an interatomic vector. In order to see this point more clearly, a spherical section of $P(\mathbf{r})$ at the Si-Si bond distance ($r=2.35$ Å) is shown in Fig. 5(b). Due to the C_{2v} symmetry of the surface and the inversion symmetry of the Patterson function, the first quadrant of the upper hemisphere is an irreducible zone, a representative of the whole $P(\mathbf{r})$. We can easily see five distinct spots in the irreducible zone in Fig. 5(b). These five spots are labeled A, U, L, B_1, and B_2, as shown in Fig. 5(c).

The radial intensity distributions of $P(\mathbf{r})$ passing through the center of each spot in Fig. 5(c) are shown in Fig. 5(d). Each radial distribution curve shows a peak at around the ideal Si-Si bond length. This supports the idea that the five distinct spots correspond to the interatomic vectors of Si-Si bonds. Since the bulk diamond structure has Si-Si bonds along the $\langle 111\rangle$ directions, one can easily assign B_1 and B_2 as the bulk bonds. The other three distinct spots A, U, and L are not along the $\langle 111\rangle$ directions; thus they are of surface origin. A unit structure of the asymmetric dimer is depicted in Fig. 6 together with the final assignments of the three distinct spots A, U, and L. Since A in Fig. 5(b) represents a bond in the xz plane, we can easily conclude that A corresponds to the asymmetric dimer bond. The other two bonds are the back bonds: U (L) corresponds to the back bond of the upper (lower) dimer atom. Thus, the observed A, U, and L are uniquely assigned as in Fig. 6.

TABLE I. The radial distances and directions of nearest neighbor bonds for the Si(001)2×1 surface as obtained from the 3D $P(\mathbf{r})$. The error is ±0.05 Å in radial distance or $\pm1°$ in angular direction.

	r (Å)	θ (deg)	ϕ (deg)
A	2.28	18	0
U	2.34	36	74
L	2.32	19	67
B_1	2.34	36	0
B_2	2.30	35	90

Since the width of the peak in the radial distribution curve in Fig. 5(d) roughly indicates the structural resolution, the structural resolution should be ~0.5 Å in the present study. However, we can determine the peak position more accurately by taking the center of the peak under the assumption that it consists of a single component. In the present study, the peak position could be determined within an accuracy of ±0.05 Å in the radial direction as well as in the polar and azimuth directions. In this connection, it is worth noting that the B_1 and B_2 spots might have multiple components that are due to the relaxation under the second layer Si. The directions and radial distances for the five spots as determined from the peak positions of $P(\mathbf{r})$ are summarized in Table I, and the resulting geometrical parameters are compared with those of previous studies in Table II. The $c(4\times2)$ translation symmetry is not taken into account in the evaluation of the present parameters. Here, we can check the accuracy or self-consistency of the bond assignments by constructing a full $c(4\times2)$ unit from the present asymmetric dimer units. Insufficient accuracy will cause a failure in joining the neighboring asymmetric dimer units. We can arrange the asymmetric dimer units to form $c(4\times2)$ periodicity with small margins of less than 0.1 Å between any bonds. Thus, the assignment is quantitatively self-consistent, and the accuracy for the interatomic vector is 0.1 Å. The accuracy is also supported by the quantitative agreement with previous studies shown in Table II: the present geometrical parameters of the dimer unit agree very well with those obtained by

TABLE II. Comparison of the geometrical parameters for the asymmetric dimer model of the Si(001)$c(4\times2)$ surface (see Fig. 6) among the present and previous studies.

	θ_d (deg)	r_d (Å)	z_u (Å)	z_l (Å)	x_s (Å)	y_u (Å)	y_l (Å)
Present	18 ± 1	2.28	1.37	0.75	3.55	3.63	4.03
Theory (Ref. 17).	18.8	2.29	1.39	0.65	3.60	3.60	4.08
PED (Ref. 19).	18.6 ± 1	2.26	1.36	0.64	3.64	3.74	3.94
SXRD (Ref. 18).	20 ± 3	2.67	1.67	0.75	3.70	3.84 [a]	3.84 [a]

[a]The ideal value was assumed (Ref. 18).

theory[17] and by photoelectron diffraction (PED).[19] Some of the parameters obtained by a recent SXRD measurement[18] are not in quantitative agreement with the others, but the assumption of unrelaxed y_u and y_l in the SXRD study might be the reason for these discrepancies.

The present high accuracy proves the validity of the Patterson (i.e., kinematical) analysis of CTDS patterns. Since the real space accuracy is related to the size of the reciprocal space surveyed in the kinematical diffraction, the accessibility of a large 3D reciprocal space by sample rotation and incident energy scan is one great advantage of CTDS in MEED. Another merit of MEED CTDS is the high surface sensitivity that is easily attainable by use of grazing incidence. It is worth noting here that the bonds in the first and second layers *A*, *U*, and *L* are imaged with comparable intensity to the bulk bonds B_1 and B_2 in Fig. 5(b).

In conclusion, the bond orientations and lengths of the nearest neighbor atoms of the asymmetric dimer unit of the Si(001)2×1 surface, have been directly reconstructed to a very high accuracy by a CTDS Patterson analysis of grazing-incidence backscattering medium-energy electron diffraction. There is no other comparable method to our knowledge to give direct information on surface geometry with such a high surface sensitivity. In actual structural analysis for an unknown surface, we might need the help of trial-and-error based surface structural analysis to assemble the building blocks into a complete surface structure. However, knowledge of the building blocks will certainly reduce the number of trial-and-error procedures. Thus, the present method should contribute greatly to surface crystallography in the future.

We thank Dr. K. Sakamoto and Dr. T. Sakamoto for providing the well-oriented Si(001) wafer. This work was partly supported by Grants-in-Aid for Scientific Research Nos. A(2) 07554051 and C(2) 11640305 and by a Creative Basic Research Grant No. 09NP1201 of the Ministry of Education, Science, Sports and Culture of Japan.

[1] J. J. Barton, Phys. Rev. Lett. **61**, 1356 (1988).
[2] D. K. Saldin and P. L. de Andres, Phys. Rev. Lett. **64**, 1270 (1990).
[3] G. R. Harp, D. K. Saldin, and B. P. Tonner, Phys. Rev. Lett. **65**, 1012 (1990).
[4] S. Y. Tong, H. Huang, and C. M. Wei, Phys. Rev. B **46**, 2452 (1992), and references therein.
[5] C. M. Wei *et al.*, Phys. Rev. Lett. **72**, 2434 (1994); K. Heinz and H. Wedler, Surf. Rev. Lett. **1**, 319 (1994).
[6] C. M. Wei, I. H. Hong, and Y. C. Chou, Surf. Rev. Lett. **1**, 335 (1994).
[7] L. D. Marks, E. Bengu, C. Collazo-Davila, D. Grozea, E. Landree, C. Leslie, and W. Sinkler, Surf. Rev. Lett. **5**, 1087 (1998).
[8] T. Abukawa, C. M. Wei, T. Hanano, and S. Kono, Phys. Rev. Lett. **82**, 335 (1999).
[9] I. Waller, Z. Phys. **17**, 398 (1923).
[10] For example, L. V. Azaroff, *Elements of X-ray Crystallography* (McGraw-Hill, New York, 1968).
[11] Z. L. Wang and J. Bentley, Ultramicroscopy **38**, 181 (1991).
[12] Z. L. Wang, Philos. Mag. B **65**, 559 (1992).
[13] Z. L. Wang, *Elastic and Inelastic Scattering in Electron Diffraction and Imaging* (Plenum Press, New York, 1995).
[14] E. Sevillano, H. Meuth, and J. J. Rehr, Phys. Rev. B **20**, 4908 (1979).
[15] D. J. Chadi, Phys. Rev. Lett. **43**, 43 (1979).
[16] R. M. Tromp, R. G. Smeenk, F. W. Saris, and D. J. Chadi, Surf. Sci. **133**, 137 (1983).
[17] A. Ramstad, G. Brocks, and P. J. Kelly, Phys. Rev. B **51**, 14 504 (1995).
[18] F. Felici, I. K. Robinson, C. Ottaviani, P. Imperatori, P. Eng, and P. Perfetti, Surf. Sci. **375**, 55 (1997).
[19] R. Gunnella, E. L. Bullock, L. Patthey, C. R. Natoli, T. Abukawa, S. Kono, and L. S. O. Johansson, Phys. Rev. B **57**, 14 739 (1998).
[20] T. Sakamoto and G. Hashiguchi, Jpn. J. Appl. Phys., Part 2 **25**, L78 (1986).
[21] T. Abukawa, T. Shimatani, M. Kimura, Y. Takakuwa, N. Muramatsu, T. Hanano, T. Goto, W. R. A. Huff, and S. Kono, J. Electron Spectrosc. Relat. Phenom. **88-91**, 533 (1998).